Dirk Mertens[1]
Claudia Heinen[2]
Edme H. Hardy[1]
Hans W. Buggisch[1]

[1] Institut für Mechanische Verfahrenstechnik und Mechanik, Universität Karlsruhe (TH), Germany.

[2] Mechanical Engineering Department, Université de Sherbrooke, Canada.

Full Paper

Newtonian and Non-Newtonian Low Re Number Flow Through Bead Packings

The results of measurements of velocity distributions of Newtonian and non-Newtonian fluids flowing through porous media are described in this contribution. The porous matrix was modeled by glass beads of different diameters forming a random bead packing confined by a circular tube. These packings were passed through by aqueous solutions of glucose and xanthane gum. Nuclear magnetic resonance (NMR) methods were applied to investigate the flow field in the packing. Spatially resolved and integral displacement distribution measurements were reported.

Keywords: Columns, Packed bed, Flow behavior, Nuclear magnetic resonance (NMR)

Received: February 2, 2006; *accepted:* May 4, 2006

DOI: 10.1002/ceat.200600048

1 Introduction

Flow through porous media is found in nature and in technology. Examples are fluid transport in plants, flow of water or oil through soil or stone, and flow of fluids in granular bed filters or catalysts. In many cases the Reynolds number characterizing the flow is low and so inertial effects may be neglected compared to forces caused by stress distribution or gravity. At the same time the Péclet number may be high, meaning that convective motion dominates over diffusive motion.

Considering Newtonian fluids, the nonlinear Navier-Stokes equations reduce to the linear ones. Consequently, the average pressure loss in a random sphere packing confined by the walls of a circular tube is proportional to the mean velocity of the flow. In these simple cases the properties of the flow field within porous matrices are well understood and also numerical simulation is possible.

Experiments on Newtonian fluid flow through porous media investigated by NMR methods are described in [1, 2]. A comparison of NMR experiments and data modeled by a three parameter approach of apparent velocities and dispersion coefficients is given in [3]. NMR data are compared with data derived from computer-generated porous matrices in (e.g., [4–6]). Another approach is to use NMR tomography data of the porous structure as input for further simulation, as described in [7]. All the above approaches show good agreement between calculated and experimental results in the case of Newtonian fluids.

With non-Newtonian fluids the situation is different due to the nonlinear relation between the tensor of strain and the tensor of deformation as well as the memory effects emerging from the viscoelastic behavior. Experiments on Newtonian and non-Newtonian fluid flow through porous matrices are described in [8] and compared to simulation results in the case of a Newtonian fluid [9]. In [10], a concept is proposed enabling the description of the flow behavior of nonlinear viscous fluids in the absence of memory effects. In most cases, however, viscoelastic effects cannot be neglected, as shown by Müller et al. [11]. Their work based on refractive index matched systems using optical methods shows a temporal fluctuation of the flow field as a critical flow rate is exceeded. Below this critical rate the flow field is dominated by viscous effects and stationary.

Considering the unsatisfactory state of knowledge in the case of non-Newtonian fluids, it seems to be worth applying methods established for Newtonian fluids to these more complex problems. While other methods like laser Doppler anemometry suffer from the necessity of optical transparency of the medium, NMR methods do not put such constraints on the sample under consideration and allow noninvasive measurement. Another advantage of NMR methods is the possibility of measurements at different timescales, making accessible the distribution functions of velocity and displacement [2]. These functions allow the characterization of the pore space geometry and the flow field. The information obtainable by NMR methods also includes information on dispersion and other transport phenomena important in process engineering. In the light of the above arguments, it is of interest to apply established NMR methods to the flow of fluids showing non-Newtonian behavior through porous media, which, to the authors' knowledge, has not been reported yet. The experi-

Correspondence: Dipl. Chem. D. Mertens (dirk.mertens@mvm.uni-karlsruhe.de), Institut für Mechanische Verfahrenstechnik und Mechanik, Universität Karlsruhe (TH), D-76128 Karlsruhe, Germany.

ments reported were performed in extension to the experiments described in [8].

2 Experimental Setup and Characterization of Bead Packings and Fluids Used

2.1 NMR Spectrometer

In the present investigation use was made of spatially resolved as well as integral nuclear magnetic resonance measurements. A Bruker Avance (DRX) NMR spectrometer and an Oxford superwide-bore superconducting magnet offering a vertical bore of 150 mm were used. The magnet supplies a magnetic induction of 4.7 T resulting in a proton Larmor precession frequency of 200 MHz. The accessible bore diameter of the magnet is reduced due to an actively shielded three axis gradient system supplying a gradient of the magnetic induction of up to 1 T/m as well as a room temperature shim system. Measurements were performed with a commercial Bruker 25 mm inner diameter birdcage resonator. Temperature was controlled by the cooling system of the gradient coils, keeping the temperature at 294 K. The flow of the different fluids was realized as gravity-driven flow, avoiding pulsations. The spectrometer was controlled by Bruker XWIN-NMR and ParaVision software [12, 13], the data being transferred to a PC for further processing. The spatially resolved velocity data was obtained using the Bruker SEVI (spin echo velocity imaging) sequence. For the integral measurements of displacement distributions the 13-interval sequence by Cotts et al. [14] was employed. Spin-density images of the water-filled packings were obtained using a RARE [1] sequence being part of the Bruker ParaVision software. Further treatment of the data was achieved using MatLab [15] and Microsoft Excel.

2.2 Flow Line and Bead Packing

A schematic representation of the experimental setup is shown in Fig. 1. A 20 mm inner diameter polyoxymethylene homopolymer (POM H) tube was used for the flow experiments.

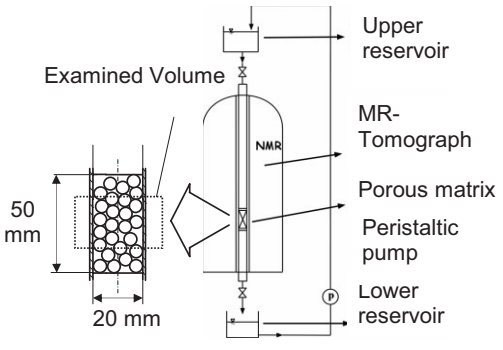

Figure 1. Experimental setup of the flow measurements. The enlarged part on the left shows the bead packing inside the flow line which is attached to the birdcage resonator inside the superconducting magnet.

Gravity-driven flow was used to minimize the effect of pulsatile flow generated by pumping. The flow rate was controlled by adjusting the difference in height of the two reservoirs. The filling level of the reservoirs was kept constant by a Marlow Watson peristaltic pump. A characterization of the glass beads can be found in [8].

2.3 Spatially Resolved Measurements

The packing was held in place by a sieve plate made from PVC with holes of 1 mm in diameter. The overall height of the packing was 50 mm. Measurement parameters such as slice thickness as well as spatial resolution are given below the figures as well as in [8]. The region under consideration is displayed in Fig. 1.

In [8], the results of measurements on mono- and polydisperse sphere packings are reported, bead diameters covering a range from 0.1 mm to 4 mm. In this work, only the results on packings of glass spheres of 1.7 mm and 4 mm will be considered. The particle size distributions of the glass beads are shown in [8]. The packings were characterized by NMR tomography acquiring spin-density images of the water-filled packing. Surface reconstructions are shown in Fig. 3 in section 3.1.

2.4 Integral Measurements

In addition to the already described potential of spatially resolved measurements on fluids streaming through porous media there exists an alternative method for examining the flow field by NMR, namely, the measurement of integral displacement distribution functions which could also be calculated from the spatially resolved results. The two major advantages of measurements without spatial resolution are the higher velocity resolution and the shorter experiment time being of the order of 20 minutes instead of hours. In contrast to the bead packing of 50 mm in height used for the spatially resolved spin echo images the propagator [16] measurements were performed on bead packings of 20 cm overall height.

2.5 Fluids

An aqueous solution of glucose (88 %) showing a dynamic viscosity of 1 Pa s at room temperature was used as Newtonian fluid. The Reynolds numbers of all flow rates used were between 10^{-3} and $5 \cdot 10^{-2}$, so inertial effects could be neglected.

Xanthane as a 0.5 % aqueous solution was used as a non-Newtonian (viscoelastic) fluid. This solution was created by adding xanthane to a 0.1 mol/dm^3 NaCl solution while stirring. To avoid degradation, 0.5 g/dm^3 $NiCl_2$ was added. The procedure for setting up a xanthane solution is described in [8]. The rheological properties of the xanthane solution used were characterized by measuring the flow curve in a cone and plate rheometer at 294 K. The resulting flow curve (taken from [8]) is shown in Fig. 2.

The maximum shear rate reached at the chosen flow rates will be of the order of magnitude of ten reciprocal seconds

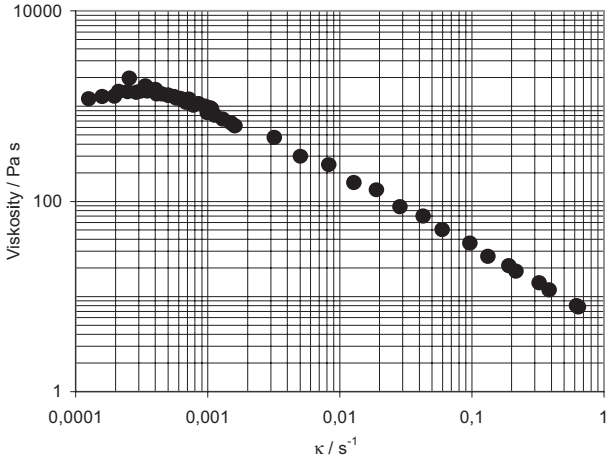

Figure 2. Flow curve of the xanthane solution used for measurements on non-Newtonian fluids. A cone and plate geometry was used at a temperature of 294 K.

leading to a dynamic viscosity between 1 and several hundred Pa s. This range of shear rates justifies the assumption of viscous effects dominating over inertial effects. On the other hand, in this shear rate regime the flow field shows pronounced viscoelastic behavior, so non-Newtonian effects are expected to be observable.

3 Experimental Results

3.1 Pore Geometry Characterized by NMR Tomography

The pore geometries of the bead packings used were characterized by NMR tomography using a RARE-3D sequence [1]. The resulting images are representations of the proton spin density in the liquid-filled packing and are presented in Fig. 3.

The images were used to calculate the radial porosity distributions shown in Figs. 4 and 5. The abscissa values are given in multiples of the bead diameter, d_p[1)]. A more detailed description of the method of calculating the porosity distributions is given in [17].

As can be concluded from comparison of Figs. 4 and 5, the variation of the radial porosity around the average porosity has almost decayed for the small glass beads of 1.7 mm diameter, while the confining effect of the wall has not decayed in the case of the 4 mm diameter glass beads. Even though this introduces wall effects, the large glass beads were used to obtain geometries manageable by the lattice Boltzmann simulations described in [9].

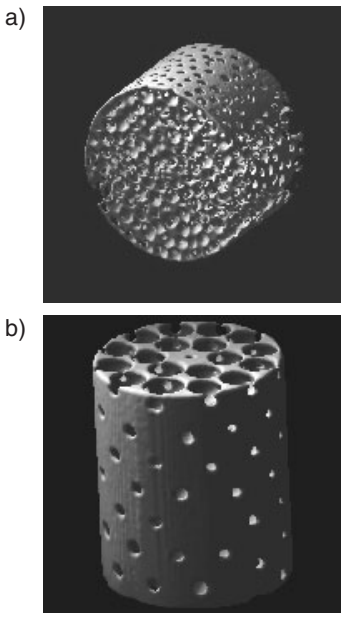

Figure 3. Spin density images of the water-filled bead packings obtained using a RARE-3D imaging sequence. (a) Beads of 1.7 mm diameter in water, imaged volume (25 mm)^3 matrix size of (128 Voxel)^3; (b) Beads of 4 mm diameter in water, imaged volume (22 mm)^3, matrix size of (128 Voxel)^3.

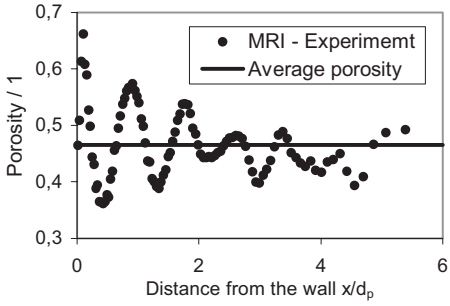

Figure 4. Porosity distributions of glass beads of 1.7 mm diameter inside a tube of 20 mm inner diameter calculated from the spin density images shown in the upper part of Fig. 3. The influence of the wall decays markedly towards the middle of the packing.

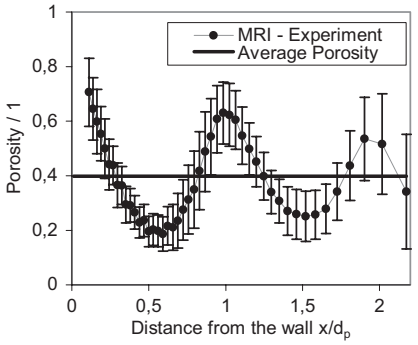

Figure 5. Porosity distributions for glass beads of 4 mm diameter inside a tube of 20 mm inner diameter calculated from the spin density images shown in the lower part of Fig. 3. The influence of the wall is still noticeable in the middle of the packing.

1) List of symbols at the end of the paper.

3.2 Velocity Profiles for Low Re Number Flow Measured by NMR

2D spatially resolved velocity profiles of a Newtonian fluid flowing through a packing of glass beads (4 mm in diameter) are shown in Fig. 6. The velocity in the main flow direction is encoded in the third dimension of the figures, the average flow velocity being $w_{avg} = 6 \cdot 10^{-4}$ ms^{-1}. The velocity profiles were measured using the Bruker SEVI sequence, a flow-compensated spin echo imaging sequence [1] supplemented by velocity encoding gradients [2]. The observation time, which means the time separating the velocity encoding gradients, was of the order of 10 ms. This short observation time as well as the low flow velocity compared to the large glass beads leads to the conclusion that the fluid elements travel a fraction of a bead diameter only and so do not significantly change their velocity. The results of the measurements are the displacement distributions which, upon division by the observation time, reflect the velocity distribution.

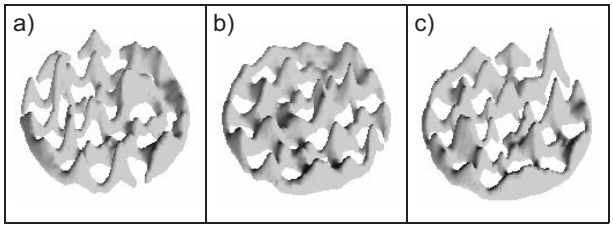

Figure 6. Spatially resolved (2D) velocity encoded images of flow velocity in the main flow direction through a bead (4 mm diameter) packing, $w_{avg} = 6 \cdot 10^{-4}$ ms^{-1}. Position: top (a), middle (b), bottom (c).

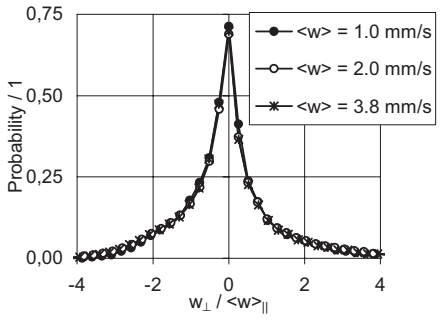

Figure 7. Velocity distribution function normal to the direction of flow for glucose solution (see [8]) calculated from the spatially resolved data and normalized by dividing the velocities by the mean axial flow velocity (lines connecting data points to guide the eye).

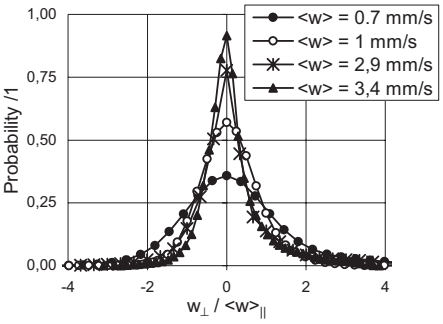

Figure 8. Velocity distribution function normal to the direction of flow for xanthane solution (see [8]) calculated from the spatially resolved data and normalized by dividing the velocities by the mean axial flow velocity (lines connecting data points to guide the eye).

The probability of velocities normal to the direction of the main flow for glucose and xanthane solution calculated by summation over the spatial coordinates is displayed in Figs. 7 and 8. Examination of Fig. 7 shows the coincidence of all the normalized traces, as expected due to the linearity of the Stokes equations. The nonlinear viscoelastic behavior of the xanthane solution reveals itself by the noncoincidence of the normalized curves in Fig. 8.

3.3 Integral Measurements of Flow and Dispersion

As an extension to the spatially resolved measurements integral propagator measurements were performed on the xanthane solution described in section 2.5. Analogous to the spatially resolved SEVI measurements gravity-driven flow through a random packing of 1.7 mm diameter glass spheres was used. The mean flow velocity was chosen to be larger than in the experiments before, extending the velocity range of the investigations. The 13-interval sequence proposed by Cotts et al. [14] was used to account for the inhomogeneous magnetic susceptibility in the matrix of the 1.7 mm diameter glass beads. Furthermore, the stimulated echo sequence allows for longer observation times. It is limited by longitudinal relaxation which can be significantly slower than the transverse relaxation limiting the observation times obtainable using the SEVI spin echo-sequence. This makes it possible to leave the regime of the velocity probability distribution function and obtain data on the displacement distribution function where fluid elements were subject to displacements of the order of the characteristic length scale of the packing, the bead diameter or even more. Finally, a better displacement resolution may be obtained in a less time-consuming way. In the following figures presenting the results of the integral measurements no distinct data points are shown as there are up to 512 data points per trace. The traces presented are the lines interconnecting the points to obtain better readability. Evaluation of the propagators was achieved by the Fourier transform of the intensity as well as phase information at the top of the stimulated echo after doubling the number of data points by zero filling once in order to increase the digital resolution. Afterwards, the data was phase corrected up to second order to minimize the imaginary part of the data. All the operations described above were applied to the raw data of the spectrometer using MatLab [15].

3.4 Measurements of Axial Non-Newtonian Flow

The propagators for different flow rates at a fixed observation time of 10 ms are displayed in Fig. 9.

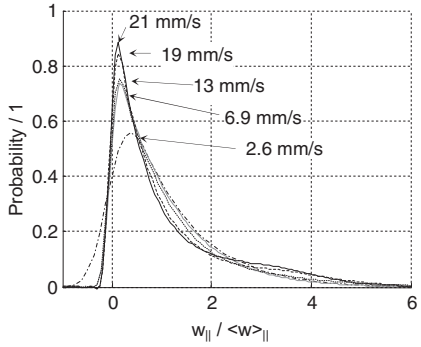

Figure 9. Propagator for an observation time of 10 ms at different flow rates clearly indicating the presence of transport opposing the main flow direction. The velocity values are normalized by dividing by the average axial velocity. Values of the propagator maxima increase with increasing velocity, indicating a lower fraction of the fluid streaming faster.

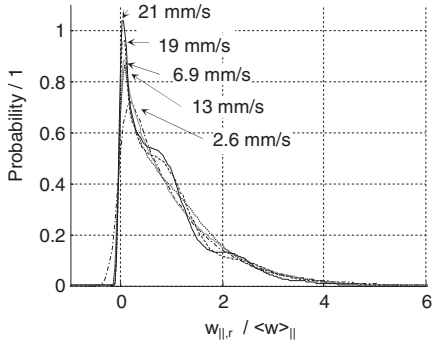

Figure 10. Propagators at different flow rates for an observation time of 50 ms leading to time averaging of the velocity, denoted by the subscript r. The velocity axis was normalized by dividing the velocity values by the average axial velocity. The sequence of the propagator maxima is the same as in Fig. 9.

As can be concluded from this figure, there is a clear indication of fluid showing negative velocities, i.e., fluid flowing upstream. For positive velocities the propagators show an approximately exponential decay. At about three times the average velocity a kind of hump forms at the highest flow rates. The shear thinning behavior of the fluid reveals itself by the shift of the propagator maxima to lower relative velocities as the flow rate increases. This means that the fraction of fast flowing spins diminishes. To check for effects the observation time and therefore the total displacement has on the propagators, the plot for measurements with an observation time of 50 ms is shown in Fig. 10.

A comparison of Fig. 9 with Fig. 10 exhibits that the effect of pronounced negative velocities at the lowest flow rate is also present at higher observation times. The sequence of the propagator maxima as well as their shift to lower relative velocities with respect to increasing average axial velocity remains the same.

An important difference between Figs. 9 and 10 is a modulation on the propagators at long observation time and high flow rate. This wavelike structure is superimposed on the distributions. An analogous behavior was reported in [16] for Newtonian fluids and referred to as 'flow diffraction'. A plot of the distribution function at constant flow rate at different observation times over the displacement reveals the wavelength of the modulation to be of the order of the bead diameter, namely, 1.7 mm. A plot of propagators obtained at different observation times and a flow rate of 21 mm/s is presented in Fig. 11.

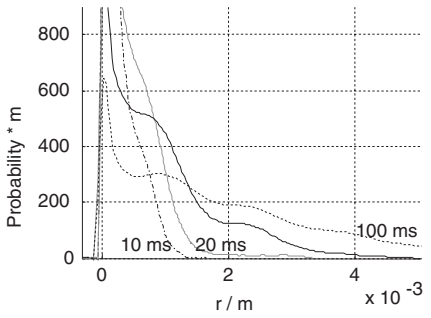

Figure 11. Propagators at varying observation time and an average flow rate of 21 mm/s showing oscillations of a wavelength correlated to the inner length scale of the packing.

From Figs. 9 and 10 it can be concluded that the wavelike modulation of the distributions can be observed as the fluid elements sample several bead diameters, be it by long observation times or high flow rates. As the observation time increases, more periods of the corresponding wave may be observed until the amplitude of the oscillation diminishes and cannot be resolved any more. After sampling several bead diameters the propagators being of a roughly exponential form starting at velocity zero in the figures presented in this report should emerge into a Gaussian distribution centered at the mean displacement. This has been shown in [3] for times of the order of five to ten times the quotient $d_p/\langle w\rangle_{||}$ and in [18]. This Gaussian distribution was not achieved in the present study due to the large glass beads used and the short longitudinal relaxation time of the fluid under consideration. The xanthane solution used in the experiments showed a longitudinal relaxation time of about 300 ms. Thus, the time required to observe the Gaussian distribution being of the order of 800 ms was clearly not obtainable using the present xanthane solution.

3.5 Measurements of Radial Non-Newtonian Flow

In addition to the velocity and displacement distributions parallel to the main flow direction measurements were performed orthogonal to that direction. As there is no net mass transport normal to the main flow, the propagators are expected to be symmetric around zero velocity or displacement. While the propagator for different flow rates plotted over velocity divided by the mean flow velocity in the main flow direction should coincide for Newtonian fluids, this is not the case for non-Newtonian fluids. This is shown in Figs. 7 and 8 taken from [8]. The measurements on xanthane solution exhibit deviations from the behavior of Newtonian fluids due to the

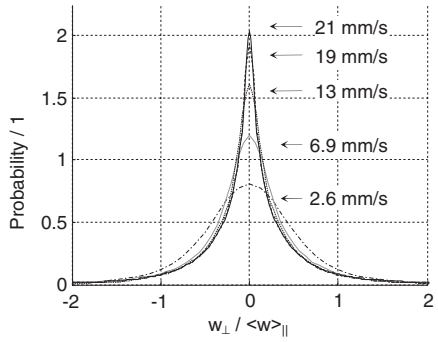

Figure 12. Velocity probability orthogonal to the main flow direction, abscissa values normalized by dividing by the mean flow velocity in the main flow direction. The observation time was 10 ms.

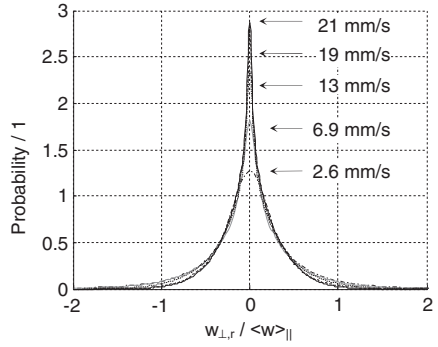

Figure 13. Velocity probability function orthogonal to the main flow direction, abscissa values normalized by dividing by the mean flow velocity in the main flow direction. The observation time was 50 ms.

nonlinear flow properties (see Fig. 8). These measurements which were made using spatially resolved spin echo techniques and summation over the spatial coordinates were extended by higher flow rates and varying observation times using stimulated echo techniques as presented in the last section [14]. The resulting propagators for different flow rates at an observation time of 10 ms are presented in Fig. 12.

At first glance it becomes obvious that the coincidence of the propagators observed examining Newtonian fluids does not exist, in agreement with the results in Fig. 8 for lower flow rates. As for the propagators presented in Fig. 9, the propagators indicate an increasing fraction of spins being of low velocity, again revealing the shear thinning behavior. The results of measurements performed at an observation time of 50 ms are presented in Fig. 13. The sequence of the propagator maxima with respect to the average velocity remains the same.

3.6 Newtonian Fluid Velocity Profiles Simulated by Lattice Boltzmann Methods

The lattice Boltzmann simulation (LBM) was performed during a cooperation with the LIST Institute of the University of Erlangen, Germany. The geometries of the 4 mm diameter bead packings measured by NMR (see Fig. 3) were used as input parameter for the simulation, making the results comparable to the NMR velocity measurements [9] revealing a good correlation between simulation and experiment. Similar results were reported by Müller et al. in [19].

4 Discussion

This report shows the results of the work on Newtonian and non-Newtonian flow through porous media. This work started with the methods described in [8], namely, spatially resolved measurements of velocity distribution functions by spin echo methods.

Inherent in the method applied (Bruker SEVI) is the inability to obtain information on the flow field at long observation times. The observation time is limited by the transverse relaxation time of the nuclei under consideration, here protons. Due to the different magnetic susceptibilities of the fluids under study compared to the glass beads forming the porous matrix, the relation $T_2 \approx T_1$, being valid in many liquids, does not hold any more, the transverse relaxation time T_2 in heterogeneous media becoming considerably shorter than the longitudinal relaxation time T_1. For this reason it is favorable to use a stimulated echo sequence limiting the observation time by longitudinal instead of transverse relaxation time.

Another feature of the stimulated echo sequence applied is the use of bipolar gradient pulses taking account of the susceptibility differences within the sample during the encoding of velocity.

As beads of 1.7 and 4 mm diameter were used, the probability distributions measured by the SEVI sequence as well as the integral stimulated echo sequence measurements of short observation time should be considered as velocity distribution functions, the observation time was of the order of 10 ms.

These short observation times as well as the low flow velocities result in displacements small compared to a bead diameter. So the term velocity distribution function is justified. Another important experimental parameter is the use of short gradient pulses of 2 ms duration, as during this time no change in velocity should occur. This is important as the velocity encoding does not compensate for higher gradient moments possibly encoding acceleration [2]. For the velocities dealt with in this report the translational motion of the spins during a gradient pulse is smaller than one bead diameter and therefore acceleration effects should not occur.

The applicability of the stimulated echo technique involving the bipolar gradient pulses was proven by measurement of the velocity distribution of laminar pipe flow. The successful reproduction of the expected top-hat propagator with the maximum velocity at twice the average velocity ensured the applicability of the phase cycle as well as gradient switching.

Comparison of the results obtained for Newtonian and non-Newtonian flow using the Bruker SEVI sequence shows some special features in the case of non-Newtonian fluid. While the expected coincidence of the velocity probability functions after normalization was achieved for the Newtonian glucose solution (see Fig. 7), this was not the case for the xanthane solution (see Fig. 8). This effect was expected due to the shear

thinning characteristics of the xanthane solution. The different probability of near zero velocities for the different flow rates applied reveals a larger fraction of spins moving at lower velocity as the flow rate increases. As shown in Figs. 12 and 13, the effect shown in Fig. 8 [8] could be reproduced employing the stimulated echo NMR measuring method. As the two different methods show the same effect for the viscoelastic fluid, it is taken for granted that this effect is not due to the measurement technique employed but characteristic of the flow of viscoelastic fluids through porous media.

Taking into consideration the pronounced occurrence of negative velocities in the probability distributions of axial velocity at the lowest flow rate, this seems to be an effect of short time fluctuations in the flow field as well as recirculation. A certain broadening of the propagator can be accounted to diffusion. Second, there could be some instabilities in the flow field of the viscoelastic fluid as reported for flow exceeding a critical flow rate [11].

Another result obtained at high flow rates and long observation times which confirms the applicability of the stimulated echo method for the measurements performed in this work is the modulation of the probability functions with the wavelength of the order of the bead diameter, an effect known as flow diffraction [16] for Newtonian fluids. To the authors' knowledge this is the first time that this effect has been reported using viscoelastic fluids.

As the longitudinal relaxation rate of the xanthane solution was too high ($R_1 \approx 3.5\ s^{-1}$) to achieve observation times required for a Gaussian distribution of velocities, no attempt was made to extract dispersion coefficients from the data obtained measuring in the direction of the flow. The occurrence of a Gaussian distribution after large displacements compared to the inner length scale of the matrix, be it achieved by high flow rates, long observation times or small characteristic length scale of the matrix, has been shown experimentally by Gibbs et al. [18] and in simulations by Packer et al. [6]. Although information on dispersion was not extracted from axial velocity measurements, dispersion coefficients depending on observation time and flow rate were obtained from the displacement distributions normal to the main flow direction. The dispersion coefficients were estimated from the full width at half maximum of the displacement distributions (see Figs. 12 and 13). For long observation times the dispersion coefficient should be independent of the observation time. As observation times were limited by relaxation and the inner length scale was too high, data did not extend to this regime of observation time independent dispersion coefficients.

5 Conclusions

In this report it was shown that NMR, be it spatially resolved or measured in an integral way, has a great potential to answer questions on the flow field in porous media. As this knowledge of the flow field in complex matrices is of outstanding importance in chemical engineering, the application of NMR methods will gain in interest in that field. It was demonstrated that the data obtained by different NMR measurement techniques lead to the same result, confirming the information obtained. The measurements of velocity distributions supply information on the flow of Newtonian and non-Newtonian fluid flow through matrices, clearly indicating the different behavior of the fluids.

The pronounced recirculation of fluid found in the flow field of the xanthane solution could also be an effect of unsteady flow behavior on the timescale of the observation time.

As respects the determination of dispersion coefficients, NMR methods are suited to provide information on these quantities, as long as the inner length scale of the matrix as well as the relaxation time of the fluids NMR active nuclei are chosen carefully.

Acknowledgements

Financial support by the DFG (FOR 338) is gratefully acknowledged. The authors would like to thank Dr. Gisela Guthausen for helpful discussions.

Symbols used

d_p	[mm]	diameter of glass beads used
R_1	[s^{-1}]	longitudinal (spin-lattice) relaxation rate ($1/T_1$)
R_2	[s^{-1}]	transverse relaxation rate ($1/T_2$)
r	[m]	displacement
T_1	[s]	longitudinal (spin-lattice) relaxation time
T_2	[s]	transverse relaxation time
$w_{\|\|}$	[m/s]	velocity in flow direction for short observation times
$w_{\|\|r}$	[m/s]	velocity in flow direction for long observation times
$<w>_{\|\|}$	[m/s]	average velocity in flow direction
$w_\perp$	[m/s]	velocity normal to flow direction for short observation times
$w_{\perp,r}$	[m/s]	velocity normal to flow direction for long observation times

Abbreviations

LBM	lattice Boltzmann method
NMR	nuclear magnetic resonance
RARE	rapid acquisition with relaxation enhancement
SEVI	spin echo velocity imaging

References

[1] E. H. Hardy, *Chem. Eng. Technol.* **2006**, *29 (7)*, 785. DOI: 10.1002/ceat200600046
[2] P. T. Callaghan, *Principles of Nuclear Magnetic Resonance Microscopy*, Clarendon Press, Oxford **1991**.
[3] M. H. G. Amin et al., *Proc. R. Soc. Lond. A* **1997**, *453*, 489.
[4] J. J. Tessier, K. J. Packer, J.-F. Thovert, P. M. Adler, *AIChE J.* **1997**, *43 (7)*, 1653.

[5] L. Lebon, J. Leblond, J. P. Hulin, *Phys. Fluids* **1997**, *9 (3)*, 481.
[6] C. De Panfilis, K. J. Packer, *Eur. Phys. J. AP* **1999**, *8*, 77.
[7] B. Manz, L. F. Gladden, P. B. Warren, *AIChE J.* **1999**, *45 (9)*, 1845.
[8] C. Heinen, MRI Untersuchungen zur Strömung Newtonscher und Nicht-Newtonscher Fluide in porösen Strukturen, *Ph.D. Thesis*, University of Karlsruhe (TH) **2004**.
[9] C. Heinen, J. Tillich, H. Buggisch, T. Zeiser, et al., *Magn. Reson. Imag.* **2005**, *23*, 369.
[10] S. Liu, J. H. Masliyah, *J. Non-Newtonian Fluid Mech.* **1999**, *86*, 229.
[11] M. Müller, J. Vorwerk, P. O. Brunn, *Rheol. Acta* **1998**, *37*, 189.
[12] XWIN-NMR Version 3.2, Bruker BioSpin GmbH, Rheinstetten, Germany, **2002**.
[13] ParaVision, Version 3.0, Bruker BioSpin MRI GmbH, Ettlingen, Germany, **2002**.
[14] R. M. Cotts, M. J. Hoch, T. Sun, J. T. Markert, *J. Magn. Reson.* **1989**, *83*, 252.
[15] Matlab, Version 7.0.0.19920 (R14), The MathWorks Inc., May 6, **2004**.
[16] J. D. Seymour, P. T. Callaghan, *J. Magn. Reson. Ser. A* **1996**, *122*, 90.
[17] V. van Buren, A. von Garnier, R. Reimert, *Chem. Eng. Technol.* **2006**, *29 (7)*, 832. DOI: 10.1002/ceat200600036
[18] J. Park, S. J. Gibbs, *AIChE J.* **1999**, *45 (3)*, 655.
[19] M. Müller, J. Vorwerk, P. O. Brunn, *Rheol. Acta* **1998**, *37*, 189.

